Metallization of Nanofilms in Strong Adiabatic Electric Fields

Maxim Durach,[1] Anastasia Rusina,[1] Matthias F. Kling,[2] and Mark I. Stockman[1,2,*]

[1]*Department of Physics and Astronomy, Georgia State University, Atlanta, Georgia 30303, USA*
[2]*Max-Planck-Institut für Quantenoptik, Hans-Kopfermann-Straße 1, D-85748 Garching, Germany*

We introduce an effect of metallization of dielectric nanofilms by strong, adiabatically varying electric fields. The metallization causes optical properties of a dielectric film to become similar to those of a plasmonic metal (strong absorption and negative permittivity at low optical frequencies). This is a quantum effect, which is exponentially size-dependent, occurring at fields on the order of 0.1 V/Å and pulse durations ranging from ~1 fs to ~10 ns for a film thickness of 3–10 nm.

The effects of strong electric fields on electron states in crystals have attracted a great deal of attention over many decades going back to Zener, who predicted a breakdown due to interband tunneling [1]. In insulators this requires electric fields on the order of atomic fields $\mathcal{E} \sim 1$–10 V/Å. Interest in strong-field condensed matter physics has recently greatly increased due to the availability of such strong electric fields in laser pulses of intensities $I \sim 10^{13}$–10^{15} W/cm^2. Ultrashort laser pulses with a few optical oscillations [2,3] open up a possibility to study ultrastrong field phenomena in solids during periods of time too short for the lattice ions to move significantly. Recent *ab initio* calculations [4] have reproduced the Zener breakdown in insulators induced by a laser pulse of intensity $\sim 10^{15}$ W/cm^2. Other strong-field phenomena that can be observable in crystals at a comparable field strength are the appearance of localized electron states, the Wannier-Stark ladder in the energy spectrum [5,6], and Bloch oscillations. [7] At orders of magnitude lower intensities, low-frequency optical fields cause a reduction of the band gap in semiconductors and insulators (Franz-Keldysh effect) [8,9]. The quantum confined Franz-Keldysh effect takes place in semiconductor quantum wells and is determined not by the field but by the total potential drop [10]. It requires typical fields $\mathcal{E} \sim 10^{-3}$ V/Å.

In this Letter, we introduce an effect of metallization in insulator nanofilms, which is predicted to occur in applied electric fields $\mathcal{E} \sim 0.1$ V/Å. It is based on adiabatic electron transfer in space across the nanofilm. The minimum duration of the field pulse required for the adiabaticity exponentially depends on the crystal thickness varying from ~1 fs for a 3 nm film to ~10 ns for a 10 nm film thickness. This metallization effect manifests itself by a dramatic change in the optical properties of the system, which start to resemble those of metals. In particular, plasmonic phenomena emerge.

To demonstrate the metallization effect, we need to solve the one-electron Schrödinger equation for a periodic potential plus a uniform electric field very accurately. We will employ the widely used Kronig-Penney model for electrons in a film confined in the x direction by an infinite

potential well. The corresponding potential energy (neglecting the electron-electron interaction) is

$$V(\mathbf{r}) = \begin{cases} U(x) + U(y) + U(z) + e\mathcal{E}x, & |x| < L/2, \\ \infty, & |x| \geq L/2, \end{cases} \quad (1)$$

where $U(x) = -\alpha \sum_{n=-\infty}^{\infty} \delta(x - na)$, and a is the lattice constant. Crystal thickness L is determined by the number of lattice periods N in the x direction: $L = Na$. Though this model does not precisely correspond to any real system, it is exactly solvable and catches the qualitative features of the strong-field phenomena from formation of the quantum bouncer (QB) states to band gap collapse and metallization transition. We use the transfer matrix to find an exact solution of the Schrödinger equation with potential (1)—see Sec. II of the supplementary material [11]. The zero boundary conditions for the wave function at $z = \pm L/2$ have been imposed and energies found semianalytically by using the shooting method.

The energy bands of the infinite crystal in the zero field are shown in Fig. 1(a) by color-coded lines for the three lowest bands: localized (green), valence (red), and conduction (blue). The discrete electronic levels for the $N = 30$ film in zero field are represented by the black dots superimposed on these infinite-crystal dispersion curves. Our computations are made for $\alpha = 13.5$ eV Å and $a = 2.7$ Å to result in the gap between the conduction and valence bands to be $E_g = 9$ eV, which is the same as for SiO$_2$. We consider an insulator (semiconductor) film where the localized and valence bands are completely filled and the conduction band is empty. This corresponds to a population of 16 electrons per unit cell (taking spin into account) and a reasonable electron density of $n = 8 \times 10^{23}$ cm^{-3}.

The energy spectrum of the nanofilm as a function of the applied field $\mathcal{E}$ normal to the film is shown in Fig. 1(b), where the filled bands are coded by green (localized band) and red (valence band), and the empty conduction band is indicated by blue. With an increase of $\mathcal{E}$, the linear Stark effect takes place, and the conduction-valence band gap decreases, completely closing at a metallization field $\mathcal{E}_m = 0.148$ V/Å indicated by the vertical dashed line. This behavior can be understood from analytical theory pre-
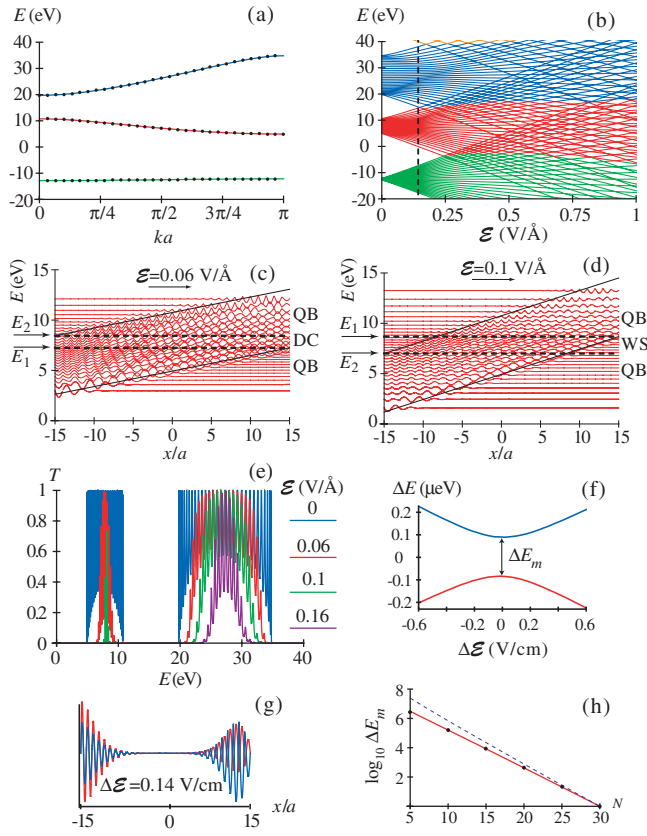
FIG. 1 (color).   Field effect on electron states: spectrum, localization, transmission, and mixing. The data are for an $N = 30$ (9 nm) nanofilm thickness. (a) Energy bands of infinite crystal (lines) and nanofilm (dots) in zero electric field. Bands are color-coded by green (localized band), red (valence band), and blue (conduction band). (b) Energy bands of nanofilm as a function of the applied electric field (color-coded as above). (c) Valence band levels in electric field $\mathcal{E} = 0.06$ V/Å. The black lines and state notations are discussed in the text. (d) The same as in (c) but for $\mathcal{E} = 0.1$ V/Å. (e) Transmission coefficient T as a function of electron energy E for different applied fields (color-coded as shown). (f) Anticrossing between the lowest-energy level in the conduction band (blue) and the highest-energy level of the valence band (red). Energy ΔE and field $\Delta \mathcal{E}$ are given with respect to the crossing point. (g) The wave functions of the anticrossing states of (f) with the corresponding color coding for $\Delta \mathcal{E} = 0.14$ V/cm. (h) The minimum splitting of the anticrossing levels as a function of the film thickness expressed as N. The black dots are obtained from numerical computation. The red line is calculated by using Eq. (4) and the dashed blue line from Eq. (5).

sented in Sec. V of the supplementary material [11], where Eq. (38) expresses $\mathcal{E}_m$ as

$$\mathcal{E}_m = \frac{E_g}{e[L - \zeta_1 \Lambda_e(\mathcal{E}_m) - \xi_1 \Lambda_h(\mathcal{E}_m)]}. \quad (2)$$

Here an electric-field quantum confinement length is $\Lambda_{e,h}(\mathcal{E}) = [\hbar^2/(2m_{e,h}^* e\mathcal{E})]^{1/3}$, where $m_{e,h}^*$ are the effective masses for electrons and holes, and ξ_1 and ζ_1 are the first roots of $\mathrm{Ai}(-x)$ and $\mathrm{Ai}'(-x)$, respectively.

The band gap can be estimated as $E_g \sim \pi^2 \hbar^2/(2ma^2)$. From this, $\Lambda_{e,h} \sim [m/(\pi^2 m_{e,h}^*)a^2 L]^{1/3} \ll L$. Neglecting $\Lambda_{e,h}$ in comparison with L, one obtains a very good approximation for $\mathcal{E}_m$, band edges $E_{b,t}$ (where b and t stand for the top and bottom, respectively), and band gap E_g as

$$\mathcal{E}_m = \frac{E_g}{eL}, \qquad E_{b,t}(\mathcal{E}) = E_{b,t} \mp e\mathcal{E}\frac{L}{2},$$
$$E_g(\mathcal{E}) = E_g - e\mathcal{E}L. \qquad (3)$$

This implies a linear Stark effect near the metallization point, in excellent agreement with Fig. 1(b).

An applied normal electric field causes the appearance of states localized between the corresponding boundary at $x = \pm L/2$ and the stopping points whose coordinates x_s and energy E are related as $E = E_{b,t} + e\mathcal{E}x_s$ [cf. Eqs. (29) and (33) of the supplementary material [11]]. These relations are represented by the slanted black lines in Figs. 1(c) and 1(d). Carriers at the conduction band bottom behave as electrons, and those at the top of the valence band behave as holes. The corresponding mobility edges are denoted as E_1 and E_2. For moderate fields [Fig. 1(c)], the states with energies $E > E_2$ or $E < E_1$ are Bloch-electron QBs [12]. The states with energies $E_2 > E > E_1$ do not have stopping points and are delocalized and conducting (DC).

For a stronger electric field, as shown in Fig. 1(d), the mobility edges overlap, $E_1 > E_2$, and the DC states disappear. Instead, localized Wannier-Stark (WS) states appear with energies $E_1 > E > E_2$. These states are very close to those in infinite lattices [6]. Their contribution to the *static* conductivity vanishes—see the next paragraph.

Assume that the barriers at the boundaries of the nanofilm are transparent enough to allow for tunneling through. Then it is meaningful to find the transmission coefficient T for carriers injected at a certain energy, which is plotted in Fig. 1(e) for the valence and conduction bands for different values of $\mathcal{E}$. As $\mathcal{E}$ increases, the transmission band collapses along with the disappearance of the DC states.

Metallic behavior is actually characterized by two different phenomena: dc conductivity and negative $\mathrm{Re}\varepsilon$ (where ε is permittivity) that contributes to plasmonic phenomena. They do not necessarily both take place simultaneously. We have shown above that the field-induced localization eliminates the dc conductivity.

Now we will show that, to the opposite, the applied field that increases slowly (adiabatically) turns an insulator crystal into a metal optically, which we call the metallization effect. The two levels at the edges of the valence and conduction band at field $\mathcal{E}_m$ experience an anticrossing as Fig. 1(f) shows. The band gap is very small: $\Delta E_m \sim 0.1$ μeV, which stems from very little overlap between the wave functions of the two edge QBs [Fig. 1(g)].

The minimum splitting of these anticrossing levels is related to the matrix element of the Zener-type tunneling between the valence and conduction bands. This splitting can be calculated analytically by using the quasiclassical approximation of Refs. [13–15] and Eq. (3). We obtain

$$\Delta E_m \propto \sqrt{\mathcal{E}_m} \exp[-\pi\sqrt{\mu E_g^3}/(4\hbar e \mathcal{E}_m)] \qquad (4)$$

$$\propto \exp[-\pi\sqrt{\mu E_g}L/(4\hbar)]/\sqrt{L}, \qquad (5)$$

where the reduced mass is $\mu = m_e^* m_h^*/(m_e^* + m_h^*)$.

The dependence of the minimum band splitting ΔE_m on $N = L/a$ from Eq. (4), where the critical field is given by Eq. (2), is shown in Fig. 1(h) with a solid red line. It is in excellent agreement with numerically computed points obtained from our quantum-mechanical solution, which are displayed as bold dots. Dependence given by a simplified expression (5) is shown by the dashed blue line in Fig. 1(h) and is a good approximation.

Now we turn to the metallization. First, consider the field $\mathcal{E} = 0.144$ V/Å, which is slightly less than $\mathcal{E}_m = 0.148$ V/Å. The corresponding energy levels near the Fermi energy $E_F \approx 14.8$ eV are shown in Fig. 2(a). We assume the temperature to be sufficiently low so only the states below E_F are occupied (shown by red) and those with $E > E_F$ are vacant (blue). The valence band states are QBs at the right boundary, and those of the conduction band are QBs at the left boundary. Though the band gap is very small, the low-frequency transitions between these two bands are drastically suppressed due to the very weak spatial overlap. This agrees with the corresponding optical spectra for $\mathcal{E} = 0.144$ V/Å shown in Fig. 3(a), which are almost the same as for $\mathcal{E} = 0$.

Assume that the field is *slowly* increased to $\mathcal{E} > \mathcal{E}_m$, so that the level anticrossing shown in Fig. 1(f) is *adiabatically* passed, which requires that the passage time $t_p \gtrsim \hbar/\Delta E_m$ (cf. Landau-Zener theory [16]). This necessitates
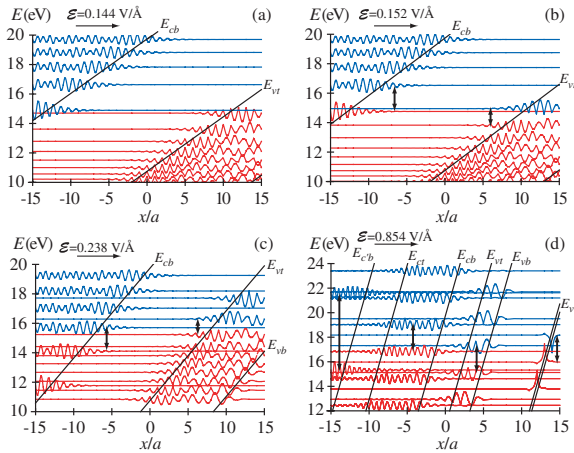
that the nanofilm is thin enough—cf. Eq. (5). Then the system persists in the ground state, and the electron population remains below the Fermi surface—see Fig. 2(b). At each boundary of the film, there are QBs on the opposite sides of the Fermi surface, which significantly overlap in space. This allows for strong electron transitions at low frequencies as shown by the vertical double arrows. Note that the transition probability between two QBs rapidly decreases with the transition frequency $\propto \omega^{-4}$ [see Eqs. (30) and (34) of the supplementary material [11]]. Correspondingly, the optical absorption is dramatically shifted to the red and IR parts of the spectrum as displayed in Fig. 3(b). In the red spectral region, Re$\varepsilon < 0$, which is characteristic of metals. This is the metallization effect.

With a further adiabatic increase of the field to $\mathcal{E} = 0.238$ V/Å, more levels cross the Fermi surface—see Fig. 2(c). A stronger low-frequency absorption takes place [Fig. 3(c)]. This signifies a more developed metallization.

For a very strong-field case illustrated in Fig. 2(d), the Fermi surface separates levels originating from four initial energy bands. The dominating transitions are those between WS states, and their frequency is $\approx e\mathcal{E}a$ increasing linearly with $\mathcal{E}$. This leads to a general shift of the optical spectra to the blue—see Fig. 3(d), where the absorption maximum is now at approximately 2 eV.

To emphasize the metallization transition, we show in Fig. 3(e) the oscillator strength f of the low-frequency (below 3 eV) transitions as a function of $\mathcal{E}$. Note that $f/n \approx 1$ is characteristic of metals. This figure demonstrates a resemblance between the metallization and a quantum phase transition. Up to the metallization critical field $\mathcal{E}_m = 0.148$ V/Å, the oscillator strength f is practically zero. After that, f increases in steps, each corresponding to a pair of QBs adiabatically crossing the Fermi surface. At the maximum, $f/n \approx 0.4$ implying that $\approx 40\%$ of the total number of electrons contributes to this metallic behavior. A further increase of $\mathcal{E}$ leads to the WS states crossing the Fermi surface and the oscillator strength decreasing [cf. Eq. (46) of the supplementary material [11]] $f \propto \mathcal{E}^{-1}$ as shown by the solid green line.

The behavior of the permittivity across the metallization transition is displayed in Fig. 3(f). Below $\mathcal{E}_m$, ε is relatively low. For $\mathcal{E} > \mathcal{E}_m$, both Re$\varepsilon(0)$ and Imε increase in steps due to the QB states crossing the Fermi surface. After reaching the maximum, the main contribution to ε shifts to the transitions between WS states originating from the same band (either valence or conduction). This causes a decrease in ε as shown by the green and orange lines computed by using Eqs. (47)–(48) of the supplementary material [11]. As the field increases, there are also transitions between the WS states originating from the different bands, leading to the sharp peaks in Fig. 3(f).

In conclusion (see also Sec. VIII of the supplementary material [11]), we have predicted an effect of metallization in dielectric nanofilms induced by an adiabatically increasing applied field. The localized states crossing the Fermi

FIG. 2 (color). Electron states in metallizing fields for $N = 30$. The occupied states (below Fermi energy E_F) are indicated by red and the vacant ones by blue. (a) Electrons in electric field $\mathcal{E} = 0.144$ V/Å slightly less than the metallization threshold $\mathcal{E}_m = 0.148$ V/Å. (b) Electrons in electric field $\mathcal{E} = 0.152$ V/Å slightly exceeding $\mathcal{E}_m$. The black double arrows denote the dominant low-frequency optical transitions. (c), (d) The same as for previous panels but for fields $\mathcal{E} = 0.238$ V/Å and $\mathcal{E} = 0.854$ V/Å, correspondingly.
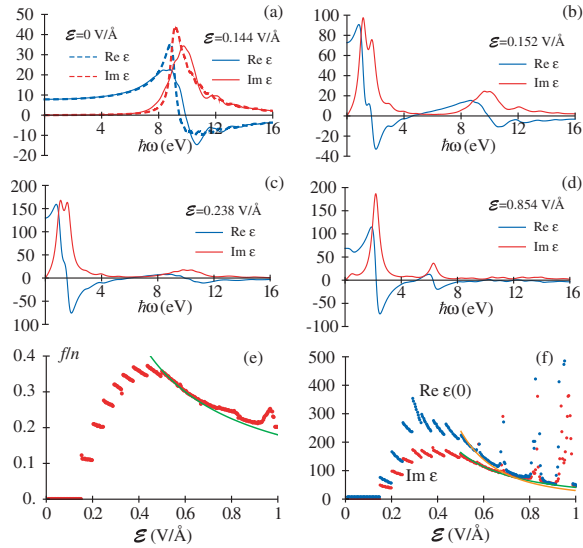
FIG. 3 (color). Optical properties of nanofilms with $N = 30$ in electric fields. (a) Below metallization threshold: real (blue) and imaginary (red) parts of permittivity ε for fields $\mathcal{E} < \mathcal{E}_m$. The dashed curves correspond to the zero field, while the solid curves are for $\mathcal{E} = 0.144$ V/Å. (b) Above metallization threshold: Reε and Imε for $\mathcal{E} = 0.152$ V/Å. Two low-frequency spectral peaks correspond to the intraband transitions between the QBs. (c) The same as in the previous panel but in a stronger field $\mathcal{E} = 0.238$ V/Å. (d) The same as (c) but for $\mathcal{E} = 0.854$ V/Å. The three low-frequency absorption peaks correspond to the Franz-Keldysh effect, intraband transitions between WS states, and intraband transition between QBs, respectively, listed in the order of increasing transition frequency. (e) Combined oscillator strength of low-frequency transitions as a function of applied electric field $\mathcal{E}$. The green line is an analytical approximation—see text. (f) The real part of dielectric permittivity at zero frequency (blue) and the imaginary part (red) of the dielectric function averaged over a low-frequency spectrum ($E < 3$ eV) as functions of the applied field. Analytical approximations (green and orange lines) are described in text.

surface cause optical absorption extending from very low (terahertz) frequencies over all optical region. In the near-IR and red spectral region, Re$\varepsilon < 0$ is predicted. This property is characteristic of metals and allows for a multitude of nanoplasmonic effects. The metallization cardinally differs from the Zener breakdown in bulk crystals, which is clear from the much lower fields required ($\mathcal{E}_m \sim 0.1$ V/Å for $L = 10$ nm). In fact, the metallization is defined not by the field $\mathcal{E}$ *per se* but by the total potential difference $\Delta U = \mathcal{E}_m L = E_g/e$. Because of the requirement of adiabatic passage to the metallized state, the rise time t_p of the applied electric field *exponentially* increases with $L\sqrt{\mu E_g}/\hbar$. For instance, for the considered case ($L = 10$ nm, $E_g = 9$ eV), $t_p \gtrsim 10$ ns, while for $L = 3$ nm the passage is much faster: $t_p \gtrsim 1$ fs.

The manifestations of the metallization depend on the way the field is induced in the nanostructure. For the excitation by an optical or terahertz wave electric field,

the metallization will cause high values of the permittivity and, consequently, bring about the plasmonic behavior of the system. This will lead, in particular, to screening of the external fields limiting the internal fields to $\mathcal{E} \sim \mathcal{E}_m$. Note that $\mathcal{E}_m \sim 0.1$ V/Å corresponds to the wave intensity $W \sim 10^{11}$–10^{12} W/cm^2, which is well tolerated by nanostructured plasmonic metals—cf. Ref. [17]. In this case, the metallization effect is completely reversible. This will open up the field of nanoplasmonics to a variety of new dielectric and semiconductor nanosystems with a plethora of new phenomena possible. Among potential applications is an ultrafast field-effect transistor where an IR or optical femtosecond pulse controls a dielectric gate.

In contrast, for a dc- to microwave-frequency potential applied via electrodes, the external potential difference is fixed. Then the metallization will lead to and is a new mechanism of the dielectric breakdown, which is fundamentally different from both the Zener and avalanche mechanisms. Such a situation is characteristic for the nanometric layers of the insulator in field-effect transistors and supercapacitors, with far-ranging technological ramifications for microelectronics and energy storage.

*mstockman@gsu.edu;
http://www.phy-astr.gsu.edu/stockman
[1] C. Zener, Proc. R. Soc. A **145**, 523 (1934).
[2] P. B. Corkum and F. Krausz, Nature Phys. **3**, 381 (2007).
[3] F. Krausz and M. Ivanov, Rev. Mod. Phys. **81**, 163 (2009).
[4] T. Otobe, M. Yamagiwa, J. I. Iwata, K. Yabana, T. Nakatsukasa, and G. F. Bertsch, Phys. Rev. B **77**, 165104 (2008).
[5] G. H. Wannier, Phys. Rev. **117**, 432 (1960).
[6] W. Shockley, Phys. Rev. Lett. **28**, 349 (1972).
[7] F. Bloch, Z. Phys. **52**, 555 (1929).
[8] W. Franz, Z. Naturforsch. A **13**, 484 (1958).
[9] L. Keldysh, J. Exp. Theor. Phys. **34**, 1138 (1958) [Sov. Phys. JETP **7**, 788 (1958)].
[10] D. A. B. Miller, D. S. Chemla, and S. Schmitt-Rink, Phys. Rev. B **33**, 6976 (1986).
[11] See supplementary material at http://link.aps.org/supplemental/10.1103/PhysRevLett.105.086803 for details of the formalism and extended results.
[12] D. M. Goodmanson, Am. J. Phys. **68**, 866 (2000).
[13] E. O. Kane, J. Phys. Chem. Solids **12**, 181 (1960).
[14] K. B. McAfee, E. J. Ryder, W. Shockley, and M. Sparks, Phys. Rev. **83**, 650 (1951).
[15] S. Glutsch, Phys. Rev. B **69**, 235317 (2004).
[16] C. Zener, Proc. R. Soc. A **137**, 696 (1932).
[17] S. Kim, J. H. Jin, Y. J. Kim, I. Y. Park, Y. Kim, and S. W. Kim, Nature (London) **453**, 757 (2008).